# Laser-induced fluorescence spectra of $Ba^{+*}$-He exciplexes produced in cold He gas

Yoshimitsu Fukuyama,[1] Yoshiki Moriwaki,[2] and Yukari Matsuo[1]
[1]*RIKEN, 2-1 Hirosawa, Wako, Saitama 351-0198, Japan*
[2]*Department of Physics, Toyama University, 3190 Gofuku, Toyama 930-8555, Japan*
(Received 9 December 2003; published 7 April 2004)

We report the observation of laser-induced fluorescence spectra of $Ba^{+*}$-He exciplexes. The experiment is carried out in an environment of cold gaseous helium at a temperature range of 3–30 K. We have observed the emission spectra of exciplexes by means of excitation of the $6p\ ^2P_{3/2} \leftarrow 6s\ ^2S_{1/2}$ transition of $Ba^+$ ions. It is found that these spectra are redshifted from the $D2$ emission line in the free space and are composed of several peaks. The experimental results are reproduced well by theoretical calculation of the emission spectra for vibrational levels of $Ba^{+*}$-He. We also investigate the vibrational dynamics of the $6p\ ^2\Pi_{3/2}$ state of $Ba^{+*}$-He, and we have determined the collision-induced vibrational relaxation cross sections of the $6p\ ^2\Pi_{3/2}$ state to be $9.7 \pm 1.1$ Å$^2$ at 15 K.

DOI: 10.1103/PhysRevA.69.042505 PACS number(s): 33.20.Kf, 34.30.+h, 34.50.Ez, 67.40.Yv

## I. INTRODUCTION

In recent years, great progress has been made in research on impurity atoms and ions in cold He environments. There have been many interesting studies on various aspects of impurity particles such as mobility of impurity ions, a snowball and a bubblelike cavity structure in liquid He, and phonon excitation and exciplex formation of impurity atoms [1]. Especially, extensive spectroscopic studies on alkali-metal atoms have revealed the formation of alkali-metal-atom–$He_n$ ($n=1,2,\ldots$) exciplexes in liquid He, in cold He gas, and on He nanodroplets [2–8]. It has been shown that the physical properties of alkali-metal-atom–$He_n$ exciplexes are characterized by the strength of the spin-orbit interaction in the $P$ state [2–5,9,10]. For heavy alkali-metal atoms (Cs), the number of He atoms binding to the alkali-metal atom in the $P$ state is restricted to two. However, for light alkali-metal atoms (Rb, K, Na, Li), the maximum number ($n_{max}$) of He atoms binding to the alkali-metal atom has been determined to be $n_{max}=6$ for Rb and K, $n_{max}>5$ for Na, and $n_{max}>3$ for Li [11].

Alkali-metal-atom–$He_n$ exciplexes of Na, K, and Rb have also been produced by means of photodetachment to the surfaces of He nanodroplets [6–8]. In addition to alkali-metal-atom–$He_n$ exciplexes, $Ag^*$-$He_n$ exciplexes in liquid He and in cold He gas have been investigated [12,13]. Exciplex formation of $Mg^*$-$He_{10}$ in liquid He has been suggested for Mg because of the considerably large redshift and broadening of the emission spectrum compared with the emission spectra of other alkaline-earth atoms [14]. On the other hand, there have been few spectroscopic studies on impurity ions in a cold He environment although the study on impurity ions in liquid He has a long history. Atkins suggested the possibility of a high-density cluster, so-called snowball, which is a dressed ion with several tens of He atoms strongly aggregated due to the monopole-induced-dipole interaction in liquid He [15]. Formation of bubbles was predicted for heavier alkaline-earth ions ($Mg^+, Ca^+, Sr^+, Ba^+$), whereas a lighter alkaline-earth ion ($Be^+$) would form a snowball [16]. These predictions have been confirmed by the results of mobility experiments [17,18]. Some alkali-metal-like ions ($Sr^+, Ba^+, Hg^+, Yb^+$) in liquid He have been observed by using spectroscopic methods [19–22]. Among these ions, only $Ba^+$ ion has shown a broad and largely redshifted emission spectrum after $D2$ excitation, which could be characteristic to an exciplex of impurity and He atoms [19]. However, to the best of our knowledge, there has been no investigation of an ionic exciplex in gas phase of He, possibly due to the experimental difficulties of producing ions in dense He gas and controlling the temperature of He gas.

In the present work, we have investigated the formation of $Ba^{+*}$-He exciplexes in cold He gas. Although alkali-metal atoms and alkaline-earth ions have the same electronic configurations, they have some different characteristics. First, alkaline-earth ions have large fine structure splittings in the $^2P$ state compared with alkali-metal atoms. A larger fine-structure splitting leads to stability of the exciplex in the $^2\Pi_{3/2}$ state against the fine-structure changing collision. Second, an alkaline-earth ion–He pair system is more attractive than an alkali-metal-atom–He pair system due to the monopole-induced-dipole interaction. In this respect, alkaline-earth ions are more suitable candidates for the observation of exciplex formation in the $^2\Pi_{3/2}$ state. In this paper, we report the first observation of $Ba^{+*}$-He exciplexes by detecting the emission spectra that have been induced by $D2$ excitation of $Ba^+$ ions in an environment of cold He gas of 3–30 K. We have also carried out theoretical calculations of the vibrational spectra of $Ba^{+*}$-He. Furthermore, we have investigated the vibrational dynamics of the $Ba^{+*}$-He exciplex and have determined the collision cross section of the vibrational relaxation in the $6p\ ^2\Pi_{3/2}$ state.

## II. EXPERIMENT

### A. Experimental overview — relevant energy-level scheme

The relevant energy-level scheme of $Ba^+$ and $Ba^{+*}$-He is shown in Fig. 1. In cold He gas, $Ba^+$ ions in the ground state are excited to the $6p\ ^2P_{3/2}$ state by irradiation of a pulsed dye laser. Excited ions in the $6p\ ^2P_{3/2}$ state are relaxed to the

 

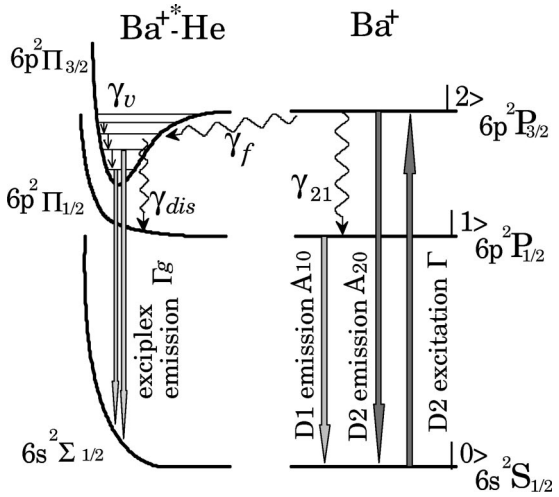


FIG. 1. Schematic energy-level diagram of $Ba^+$ and $Ba^{+*}$-He.

ground state of $6s\ ^2S_{3/2}$ through four processes. In the first process (process I), a $Ba^{+*}$-He exciplex in the $6p\ ^2\Pi_{3/2}$ state is formed of a $Ba^+$ ion in the $6p\ ^2P_{3/2}$ state and two He atoms due to a three-body collision, and the $Ba^{+*}$-He exciplex is deexcited directly to the $6s\ ^2\Sigma_{1/2}$ state by emitting fluorescence. The $Ba^{+*}$-He exciplex in the $6s\ ^2\Sigma_{1/2}$ state immediately dissociates to a $Ba^+$ ion in the ground state and a He atom in the ground state because of the repulsive feature of $Ba^+$-He potential in the $6s\ ^2\Sigma_{1/2}$ state. In the second process (process II), an ion in the $6p\ ^2P_{3/2}$ state is deexcited directly to the ground state by emitting a photon ($D2$ emission). In the third process (process III), an ion in the $6p\ ^2P_{3/2}$ state is deexcited to the $6p\ ^2P_{1/2}$ state due to the fine-structure changing collision, and the ion is subsequently deexcited to the ground state by emitting a photon ($D1$ emission). In the fourth process (process IV), the $Ba^{+*}$-He exciplex in the $6p\ ^2\Pi_{3/2}$ state formed in the former half of process I is deexcited into the $6p\ ^2\Pi_{1/2}$ state, where there is no bound state for a $Ba^+$-He pair, due to a collision of $Ba^+$-He with a He atom and subsequently dissociates into a $Ba^+$ ion in the $6p\ ^2P_{1/2}$ state and He atoms in the ground state. Then, the $Ba^+$ ion in the $6p\ ^2P_{1/2}$ state is deexcited to the ground state with $D1$ emission.

### B. Experimental apparatus

The experimental setup and a typical time chart are illustrated in Fig. 2. The experimental apparatus consists of a cryostat chamber, ablation laser, excitation laser, and detection system. The cryostat chamber contained liquid He in the bottom part. The space above the liquid He was filled with cold He gas. By adjusting both conductance of He gas pumping and evaporation of liquid He by a heater immersed in liquid He, we were able to control the temperature and the pressure of cold He gas independently in the experimental region of the cryostat chamber. The temperature was measured by a commercial temperature sensor (Lake Shore, Cernox CX-1050-AA) with an accuracy of 0.1 K. The pressure of He gas was monitored with a capacitance manometer (MKS Baratron). A small piece of solid Ba sample was

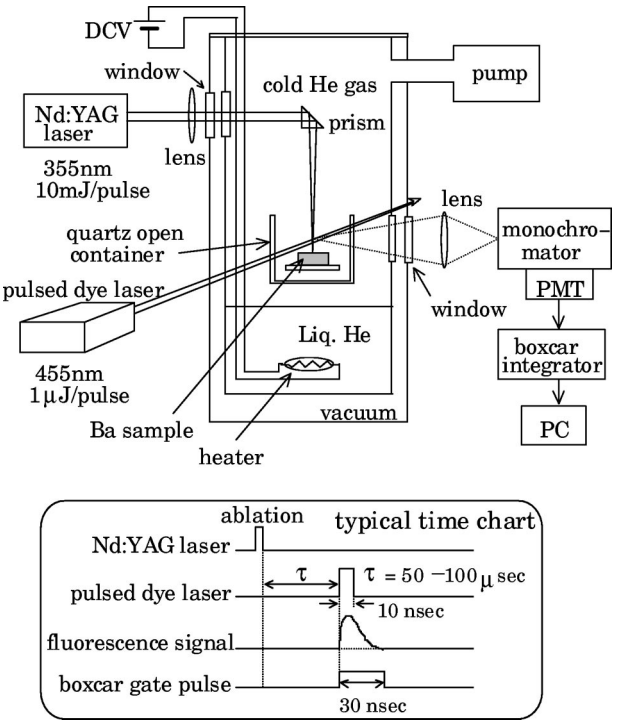


FIG. 2. Experimental setup and typical time chart.

placed in a quartz open container, which was fixed above the liquid level, to prevent the disturbance of direct He gas flow. Barium ions were produced in the cold He gas by ablating the solid Ba sample with the third harmonic pulse of Nd:YAG (yttrium aluminum garnet) laser output (New Wave, Tempest, 355 nm, pulse duration 8 ns). The pulse energy was $\approx$10 mJ/pulse and repetition rate was 5 Hz. The number of ablated ions depends on the power density of the ablation laser, the surface condition of the solid Ba sample, and the pressure of cold He gas. Typically, $10^{10}$ ions were dispersed into cold He gas. Then the $Ba^+$ ions were irradiated by a pulsed dye laser (Lambda Physik, FL30002, pulse duration 15 ns, $\approx$1 $\mu$J/pulse), which was tuned to the $D2$ line with a 50–100 $\mu$s delay time from the laser ablation pulse. The pulsed dye laser beam was aligned 5 mm above the solid Ba sample and the diameter was about 4 mm. Laser-induced fluorescence from ions and exciplexes was detected with a photomultiplier tube (Hamamatsu, R955) through a 25 cm grating monochromator (Jasco, CT25), and the signal was averaged with a boxcar integrator (Stanford Research SR250) and stored in a computer. The gate pulse duration of the boxcar integrator was set to 30 ns.

## III. CALCULATION OF EMISSION SPECTRA OF $Ba^{+*}$-He

In order to discuss the experimental emission spectra of $Ba^+$ in cold He gas, we have carried out model calculations to reproduce the emission spectra. In this model calculation, we first obtained interaction potentials for the $6s\Sigma$, $6p\Sigma$, and $6p\Pi$ states of a $Ba^+$ ion and a He atom pair from *ab initio* calculations using the program package MOLPRO [23]. The details of the calculation will be published elsewhere [24]. Then we introduced the spin-orbit interaction with a form of

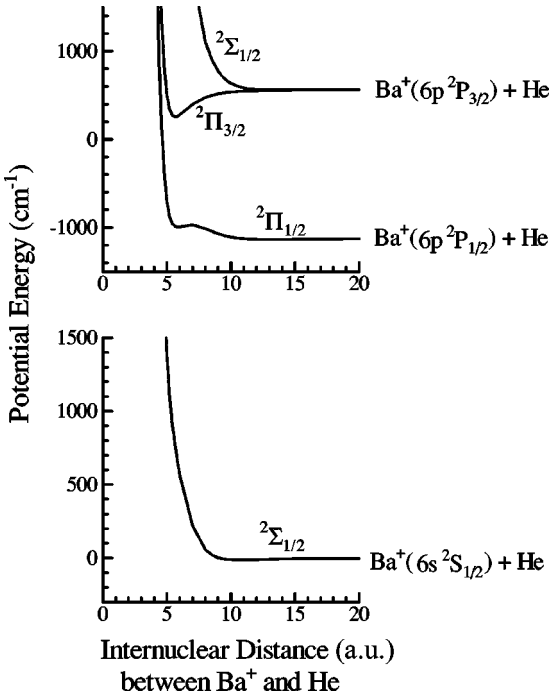


FIG. 3. Adiabatic potential curves of a $Ba^{+*}$-He pair.

$V=\frac{2}{3}\Delta_{so}\boldsymbol{l}\cdot\boldsymbol{s}$, where $\Delta_{so}$ is the spin-orbit splitting energy of $Ba^+$ in the $6p\ ^2P$ states, and $\boldsymbol{l}$ and $\boldsymbol{s}$ are the angular momentum and spin operator of the valence electron, respectively. Finally, by diagonalizing the Hamiltonian, interatomic potentials for the $6s\ ^2\Sigma_{1/2}$, $6p\ ^2\Sigma_{1/2}$, $6p\ ^2\Pi_{1/2}$, and $6p\ ^2\Pi_{3/2}$ states were obtained. The results are shown in Fig. 3. The potential curve for the $6p\ ^2\Pi_{3/2}$ state has a well at an internuclear distance of 5.7 a.u. with a depth of 330 cm$^{-1}$ from the dissociation limit. Eigenenergies of vibrational levels were calculated for this potential curve. The results are listed in Table I. We calculated the emission spectrum of the transitions from all the vibrational levels to the ground $6s\ ^2\Sigma_{1/2}$ state using the spectral method based on the Franck-Condon principle [25]. The results are shown in Fig. 4.

TABLE I. Calculated vibrational eigenenergies of $Ba^{+*}$-He in the $6p\ ^2\Pi_{3/2}$ state together with the centers and the widths (FWHM) of the four main peaks for the calculated and observed emission lines. Vibrational energies are given relative to the energy of the dissociation limit of $Ba^+(6p\ ^2P_{3/2})+He$.

| | | Emission lines (cm$^{-1}$) | | | |
|---|---|---|---|---|---|
| Vibrational | Vibrational | Calculated | | Observed | |
| level | energy (cm$^{-1}$) | Center | Width | Center | Width |
| $v=0$ | −244 | 21058 | 576 | 20910 | 380 |
| $v=1$ | −144 | 21542 | 384 | 21280 | 220 |
| $v=2$ | −81 | 21805 | 200 | 21550 | 160 |
| $v=3$ | −36 | 21922 | 40 | 21770 | 91 |
| $v=4$ | −13 | | | | |
| $v=5$ | −3.4 | | | | |

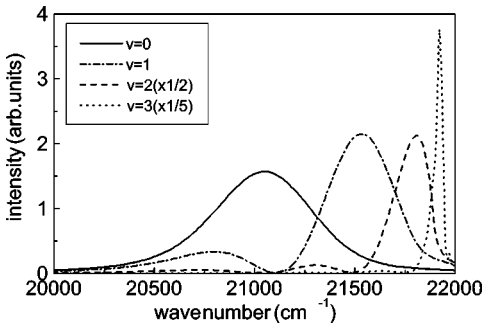


FIG. 4. Calculated emission spectra from the $6p\ ^2\Pi_{3/2}$ state to the $6s\ ^2\Sigma_{1/2}$ state of $Ba^{+*}$-He. Intensity of the calculated emission line from each vibrational level is normalized to its total photon energy.

## IV. RESULTS AND DISCUSSION

### A. Emission spectra induced by *D*2 excitation

We observed laser-induced fluorescence spectra of $Ba^+$ in cold He gas by means of $D2$ excitation of $Ba^+$ (21 952 cm$^{-1}$). A typical spectrum observed at the temperature of 25 K and pressure of 6700 Pa is shown in Fig. 5. The observed spectrum is composed of a sharp line of $D1$ transition of $Ba^+$ at 20 262 cm$^{-1}$ and a broad fluorescence band over a range of 20 500−21 800 cm$^{-1}$. No emission spectrum of $D2$ could be recorded since the scattering light from the $D2$ excitation laser completely masked the $D2$ emission light. The broad fluorescence band was observed only in the temperature and pressure ranges of 3−30 K and 2000−27 000 Pa, respectively. We assigned this broad fluorescence band to the $6p\ ^2\Pi_{3/2}\rightarrow 6s\ ^2\Sigma_{1/2}$ transition of the $Ba^{+*}$-He exciplex as discussed in the following.

The broad fluorescence band is decomposed into four components. We approximated each component as a Gaussian for simplicity and fit the broad fluorescence spectrum to the superposition of four Gaussian curves. Centers and full widths at half maximum (FWHM) are listed in Table I. Reasonably good agreement between the observed and calculated emission spectra suggests that these four components are transitions from the vibrational levels ($v=0,1,2$, and 3) in the $6p\ ^2\Pi_{3/2}$ state of the $Ba^{+*}$-He exciplex to the ground state. Although the theoretical calculation predicts there are six vibrational levels in the $6p\ ^2\Pi_{3/2}$ state, emissions from

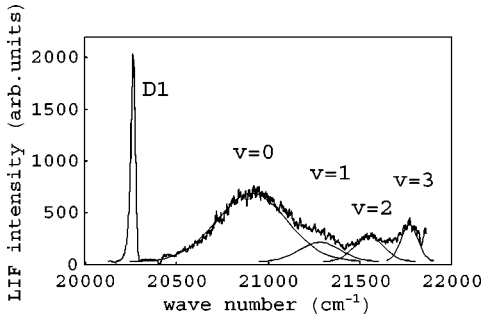


FIG. 5. Laser-induced fluorescence spectra of $Ba^+$ ions and $Ba^{+*}$-He exciplexes (thick line). Thin lines correspond to four vibrational peaks approximated with Gaussian curves.

vibrational levels $v=4$ and 5 were not observed due to the strong scattering light of the $D2$ excitation laser. It should be noted that the centers of the observed emission lines from vibrational levels of the $6p\ ^2\Pi_{3/2}$ state are shifted about $150-250\ \mathrm{cm}^{-1}$ to the red side compared with those of the predicted ones. The widths of those observed emission lines are narrower than the predicted ones except for the case of transition from the $6p\ ^2\Pi_{3/2}\ v=3$ state.

Emission from the $6p\ ^2\Pi_{3/2}$ state of $Ba^{+*}$-He induced by $D1$ excitation was not observed because of the large fine-structure splitting ($1690\ \mathrm{cm}^{-1}$) of $Ba^+$. Emission from the $6p\ ^2\Pi_{1/2}$ state of $Ba^{+*}$-He was also not observed by either $D1$ or $D2$ excitation because there is no bound state in the $6p\ ^2\Pi_{1/2}$ state of the $Ba^+$-He pair. According to the experimental observation of $Ba^+$ implanted in liquid He, we expected a broad fluorescence band of $Ba^{+*}$-$He_2$ exciplexes appearing around $19\,900\ \mathrm{cm}^{-1}$. Although we searched $Ba^{+*}$-$He_2$ emission over a frequency region from 17 000 to $22\,000\ \mathrm{cm}^{-1}$, it was not detected with the sensitivity of our experimental apparatus. This is because the number density of cold He gas in our experimental condition ($\sim 10^{19}\ \mathrm{atoms/cm}^3$) was about $10^3$ times smaller than that of liquid He, so that the production rate of $Ba^{+*}$-$He_2$ should be quite small.

The laser-induced fluorescence spectra of $Ba^+$ ions after $D2$ excitation in cold He gas are similar to those of Cs atoms [11]. Both emission spectra of the $6p\ ^2\Pi_{3/2} \rightarrow 6s\ ^2\Sigma_{1/2}$ transitions of $Ba^{+*}$-He and $Cs^*$-He exciplexes are broad and are redshifted from the $D2$ emission line in the free space, and they are composed of several peaks. This is reasonable considering that $Ba^+$ and Cs have the same electronic configurations of valence electrons. However, the redshift for $Ba^+$ ($1050\ \mathrm{cm}^{-1}$) is quantitatively different from that for Cs ($700\ \mathrm{cm}^{-1}$). Moreover, as the vibrational level becomes higher, the linewidth (FWHM) of the vibrational level for $Ba^{+*}$-He decreases more rapidly than that in the case of $Cs^*$-He. These quantitative differences in emission spectra are considered to be caused by the shapes of $Ba^+$-He and Cs-He interaction potentials. An alkaline-earth-ion–He pair system is more attractive than an alkali-metal-atom–He pair system due to the monopole-induced-dipole interaction, thus the depth of the potential curve well in the $6p\ ^2\Pi_{3/2}$ state of a $Ba^+$-He pair is three times greater than that of a Cs-He pair. The large redshift of $Ba^{+*}$-He can be mainly explained by the deep potential well in the $6p\ ^2\Pi_{3/2}$ state of a $Ba^+$-He pair. In the case of a $Ba^+$-He pair, the potential well in the $6p\ ^2\Pi_{3/2}$ state is wide and the potential curve in the $6s\ ^2\Sigma_{1/2}$ state is gentle in the vicinity of the minimum energy of the $6p\ ^2\Pi_{3/2}$ state, whereas the well of Cs-He is narrow and steep. Therefore, the linewidth for $Ba^{+*}$-He should be rapidly reduced as the vibrational level becomes higher. We conclude that the quantitative differences in emission spectra for $Ba^{+*}$-He and $Cs^*$-He exciplexes can be explained by the shapes of interatomic potentials of $Ba^+$-He and Cs-He pairs.

The observed $D1$ emission line can be generated by two independent processes (process III and process IV, as noted in Sec. II A). In process III, a $Ba^+$ ion in the $6p\ ^2P_{3/2}$ state is deexcited to the $6p\ ^2P_{1/2}$ state due to the fine-structure changing collision and is then deexcited into the ground state radiating $D1$ emission. In process IV, a $Ba^{+*}$-He exciplex in the $6p\ ^2\Pi_{3/2}$ state is deexcited into the $6p\ ^2\Pi_{1/2}$ state due to a collision with a He atom and subsequently dissociates into a $Ba^+$ ion in the $6p\ ^2P_{1/2}$ state and a He atom in the ground state, and then the $Ba^+$ ion is deexcited to the ground state by emitting a photon ($D1$ emission). It is known that the fine-structure changing collision rate of $Ba^+$ from the $6p\ ^2P_{3/2}$ state to the $6p\ ^2P_{1/2}$ state depends linearly on the He gas density up to 93 000 Pa at room temperature [24]. On the other hand, the population transfer rate due to process IV is considered to be proportional to the square of He gas density because the $Ba^{+*}$-He exciplex is produced by a three-body collision. In order to investigate the behavior of processes III and IV at low temperature, we carried out an additional experiment at various He gas densities and evaluated the fine-structure changing collision rate and population transfer rate by processes III and IV at the temperature of 20 K or lower. Our experimental results showed that the relaxation rate is proportional to the square of He gas density. Thus, we conclude that process IV is dominant rather than process III for the $Ba^+$-He system in the low-temperature region below 20 K. The relaxation process of the $Ba^+$-He system will be reported in detail elsewhere [26].

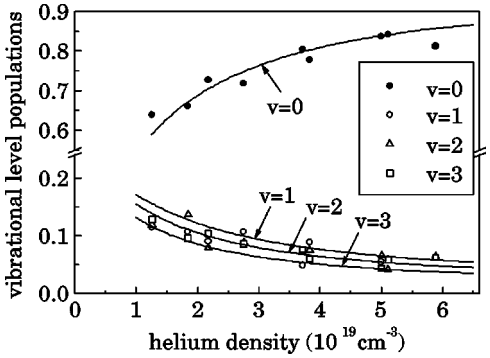


FIG. 6. Vibrational level populations in the $6p\ ^2\Pi_{3/2}$ state of $Ba^{+*}$-He. Solid lines represent the fitting results of the time evolution of Eqs. (1).

It would be interesting to investigate processes III and IV for a $Sr^+$-He pair system in cold He gas, because the fine-structure splitting of $Sr^+$ ($801\ \mathrm{cm}^{-1}$) is two times smaller than that of $Ba^+$, and the fine-structure changing cross section of $Sr^+$ is almost two orders of magnitude larger than that of $Ba^+$ at room temperature [24,27]. In a preliminary experiment, we found that laser-induced fluorescence of $Sr^{+*}$-He exciplexes is induced by $D2$ excitation in the temperature and pressure ranges of 5–15 K and 10 000–20 000 Pa, respectively. Further work on $Sr^{+*}$-He is in progress.

### B. Vibrational level populations of $Ba^{+*}$-He

In this section, we discuss the relative vibrational level populations in the $6p\ ^2\Pi_{3/2}$ state of $Ba^{+*}$-He in the temperature range of 10–20 K. By fitting a broad fluorescence spectrum to the superposition of four Gaussian curves as described in the preceding section, the vibrational level populations were evaluated for He gas densities ranging from $1\times10^{19}$ to $6\times10^{19}\ \mathrm{atoms/cm}^3$, as shown in Fig. 6. It should be noted that the relative vibrational level population

was normalized to the sum of $v=0,1,2$, and 3 vibrational level populations because we could not observe emission from $v=4$ and 5 levels. In the He gas density range used in our experiment, the emission from the $v=0$ vibrational level always gives the largest intensity, indicating that the majority of the population is in the $v=0$ vibrational level. It was also found that vibrational level populations in the $6p\ ^2\Pi_{3/2}$ state depend on He gas density but not on He pressure or temperature. As the He gas density increases, the population of the $v=0$ vibrational level increases slightly, whereas the populations of the $v=1,2$, and 3 vibrational levels decrease. There is no significant difference among the populations of $v=1,2$, and 3 vibrational levels in the $6p\ ^2\Pi_{3/2}$ state.

We have taken three relaxation processes into account to evaluate the population of the $6p\ ^2\Pi_{3/2}$ state of $Ba^{+*}$-He: the relaxation among the vibrational levels in the $6p\ ^2\Pi_{3/2}$ state (rate $\gamma_v$), the relaxation between the $6p\ ^2\Pi_{3/2}$ and $6p\ ^2\Pi_{1/2}$ states (rate $\gamma_{dis}$), and the radiative relaxation of the $6p\ ^2\Pi_{3/2}$ state (rate $A'_{exci}$). In order to explain the experimental results, we have simulated the vibrational populations in the $6p\ ^2\Pi_{3/2}$ state based on the rate equations of six vibrational levels ($v=0,1,\ldots,5$) of $Ba^{+*}$-He and the $6p\ ^2P_{3/2}$ state of $Ba^+$. When the $6p\ ^2P_{3/2}$ state is populated by $D2$ excitation with the time-varying pumping rate $\Gamma$, the rate equations are as follows (see Fig. 1):

$$\begin{aligned}\dot{n}_2 &= \Gamma\ n_0 - (A'_2 + \gamma_f)n_2,\\ \dot{n}_{v_i} &= \gamma_{f_i} n_2 + \gamma_v n_{v_{i+1}} + \gamma'_{v_{i-1}} n_{v_{i-1}}\\ &\quad - (A'_{exci} + \gamma_{dis} + \gamma_v + \gamma'_{v_i}) n_{v_i} \quad (i = 0, \ldots, 5),\end{aligned} \tag{1}$$

where $n_2$, $n_0$, and $n_{v_i}$ represent the number densities of $Ba^+$ in the $6p\ ^2P_{3/2}$ state and in the $6s\ ^2S_{1/2}$ state, and that of $Ba^{+*}$-He in the vibrational level $i$ ($n_{v_6}=0$), respectively. $A'_2$ is the radiative relaxation rate of the $6p\ ^2P_{3/2}$ state of $Ba^+$. The rate $\gamma_f$ is the exciplex formation rate due to a three-body collision of a $Ba^+$ ion in the $6p\ ^2P_{3/2}$ state and two He atoms, and we assume that the formed exciplexes populate equally in all vibrational levels ($\gamma_{f_i}=\gamma_f/6$). The rate $\gamma'_{v_i}$ is the collision excitation rate from the vibrational level $i$ to $i+1$ in the $6p\ ^2\Pi_{3/2}$ state of $Ba^{+*}$-He. The detailed balance is assumed for the collision excitation rate $\gamma'_{v_i}=\gamma_v \exp[-(E_{i+1}-E_i)/kT]$, where $E_i$ is the energy of the $i$th vibrational level. We assume for simplicity that the rates $A'_{exci}$, $\gamma_{dis}$, and $\gamma_v$ do not depend on the vibrational level $i$. The cross sections of exciplex formation $\sigma_f$, dissociation $\sigma_{dis}$, and vibrational relaxation $\sigma_v$ are expressed by the relations

$$\gamma_f = n_{\mathrm{He}}^2 v_{\mathrm{He}} \sigma_f, \quad \gamma_{dis} = n_{\mathrm{He}} v_{\mathrm{He}} \sigma_{dis}, \quad \gamma_v = n_{\mathrm{He}} v_{\mathrm{He}}\ \sigma_v, \tag{2}$$

where $v_{\mathrm{He}}$ is the relative mean velocity of He-$Ba^+$ or He–$Ba^{+*}$-He.

The cross sections of exciplex formation $\sigma_f$ and dissociation $\sigma_{dis}$ are given by $\sigma_f = 0.207 \pm 0.014 \times 10^{-45}$ m$^5$ and $\sigma_{dis} = 0.171 \pm 0.010$ Å$^2$ at 15 K [26]. The decay rate of $Ba^{+*}$-He in the $6p\ ^2\Pi_{3/2}$ state ($A'_{exci}+\gamma_{dis}$) has been determined to be $1.28 \pm 0.08 \times 10^8$ s$^{-1}$ by fitting the time-dependent fluorescence profile of $Ba^{+*}$-He to the convolution of the excitation laser profile and exponential decay curve. The value of $A'_2$ is $1.585 \times 10^8$ s$^{-1}$ [28].

The vibrational relaxation rate $\gamma_v$ in the $6p\ ^2\Pi_{3/2}$ state of $Ba^{+*}$-He is obtained as a fitting parameter in the time evolution of rate equations (1). Calculated values of relative population of vibrational levels are also shown in Fig. 6. It should be noted that the total population of $v=0,1,2$, and 3 levels is normalized to unity. Good agreement between the experimental data and fitting curves supports the validity of our assumption that three cross sections $\sigma_f$, $\sigma_{dis}$, and $\sigma_v$ and the radiative relaxation rate $A'_{exci}$ do not depend on vibrational levels in the $6p\ ^2\Pi_{3/2}$ state. Using Eqs. (2), the cross section of vibrational relaxation $\sigma_v$ is determined to be $9.7 \pm 1.1$ Å$^2$ at 15 K.

It is well known that the vibrational relaxation rate decreases as temperature increases in a range of low temperatures in which the long-range attractive force controls vibrational relaxation processes [29]. In a range of high temperatures in which the short-range repulsive force governs collision processes, the vibrational relaxation rate increases as temperature increases. The minimum point of the relaxation rate appears around the temperature that corresponds to interaction well depth of a molecular ion and a collision partner [30,31]. This has been clearly demonstrated in a few cases, most notably for the $O_2^+$-Kr system [30] and the $NO^+$-$CH_4$ system [31]. However, experimental data obtained at room temperature or at lower temperature are scarce since vibrational relaxation processes have been studied mostly at high temperature. Among them, the vibrational relaxation rate of an $NO^+X$ ($v=1$) state due to a collision with a He atom has been determined to be $k_q = 1 \times 10^{-10}$ cm$^3$ s$^{-1}$ at 1 K [29]. On the other hand, the vibrational quenching rate of $NO^+$ ($v=1,4$) by Ar collisions at room temperature lies in the range of $10^{-14}$–$10^{-12}$ cm$^3$ s$^{-1}$ [32]. Our experimental value for the vibrational relaxation rate of $Ba^{+*}$-He corresponds to $2.97 \times 10^{-11}$ cm$^3$ s$^{-1}$ at 15 K. This value is on the slope of negative temperature dependence because the interaction well depth of a $Ba^{+*}$-He–He system is ≈480 K. It would be interesting to investigate in detail the temperature dependence of vibrational relaxation over the temperature range from 1 K to several tens of Kelvin in a future work.

## V. CONCLUSIONS

We have observed laser-induced fluorescence of $Ba^{+*}$-He exciplexes ($6p\ ^2\Pi_{3/2} \rightarrow 6s\ ^2\Sigma_{1/2}$) in cold He gas in a temperature range of 3–30 K. The emission spectra of $Ba^{+*}$-He induced by $D2$ excitation are broadened and are redshifted from the $D2$ emission line of $Ba^+$. The broad emission band of $Ba^{+*}$-He is composed of four components, which are assigned to be transitions from different vibrational levels ($v=0,1,2$, and 3) in the $6p\ ^2\Pi_{3/2}$ state to the bound-free $6s\ ^2\Sigma_{1/2}$ state. We have also performed *ab initio* calculations to determine the pair potential of a $Ba^{+*}$-He system and have calculated emission spectra based on the

Franck-Condon approximation. The observed emission spectra of $Ba^{+*}$-He are in reasonably good agreement with calculated ones. The vibrational level populations in the $6p\ ^2\Pi_{3/2}$ state of $Ba^{+*}$-He were reproduced well by rate equation analysis. The cross section of vibrational relaxation in the $6p\ ^2\Pi_{3/2}$ state is determined to be $\sigma_v = 9.7 \pm 1.1$ Å$^2$ at 15 K. Experiments on $Sr^{+*}$-He exciplexes in cold He gas are also in progress. The details will be reported elsewhere.

**ACKNOWLEDGMENTS**

We would like to thank Dr. Tohru Kobayashi of RIKEN for his help in the experiment. One of the authors (Y.F.) acknowledges support from RIKEN. This work was partly supported by a Grant-in-Aid for Scientific Research from the Ministry of Education, Science, Sports and Culture.

[1] Z. Phys. B: Condens. Matter **98**, 297 (1995), special issue on ions and atoms in superfluid helium, edited by H. Günther and B. Tabbert.
[2] T. Kinoshita, K. Fukuda, Y. Takahashi, and T. Yabuzaki, Phys. Rev. A **52**, 2707 (1995).
[3] T. Kinoshita, K. Fukuda, T. Matsuura, and T. Yabuzaki, Phys. Rev. A **53**, 4054 (1996).
[4] K. Enomoto, K. Hirano, M. Kumakura, Y. Takahashi, and T. Yabuzaki, Phys. Rev. A **66**, 042505 (2002).
[5] K. Hirano, K. Enomoto, M. Kumakura, Y. Takahashi, and T. Yabuzaki, Phys. Rev. A **68**, 012722 (2002).
[6] J. Reho, J. Higgins, C. Callegari, K. K. Lehmann, and G. Scoles, J. Chem. Phys. **113**, 9686 (2000).
[7] C. P. Schulz, P. Claas, and F. Stienkemeier, Phys. Rev. Lett. **87**, 153401 (2001).
[8] F. R. Brühl, R. A. Trasca, and W. E. Ernst, J. Chem. Phys. **115**, 10 220 (2001).
[9] J. Dupont-Roc, Z. Phys. B: Condens. Matter **98**, 383 (1995).
[10] J. Pascale, Phys. Rev. A **28**, 632 (1983).
[11] K. Enomoto, K. Hirano, M. Kumakura, Y. Takahashi, and T. Yabuzaki, Phys. Rev. A **69**, 012501 (2004).
[12] J. L. Persson, Q. Hui, Z. J. Jakubek, M. Nakamura, and M. Takami, Phys. Rev. Lett. **76**, 1501 (1996).
[13] Z. J. Jakubek, Q. Hui, and M. Takami, Phys. Rev. Lett. **79**, 629 (1997).
[14] Y. Moriwaki and N. Morita, Eur. Phys. J. D **5**, 53 (1999).
[15] K. Atkins, Phys. Rev. **116**, 1339 (1959).
[16] M. W. Cole and R. A. Bachman, Phys. Rev. B **15**, 1388 (1977).
[17] H. Günther, M. Foerste, M. Kunze, G. zu Putlitz, and U. von Stein, Z. Phys. B: Condens. Matter **101**, 613 (1996).
[18] M. Foerste, H. Günther, O. Riediger, J. Wiebe, and G. zu Putlitz, Z. Phys. B: Condens. Matter **104**, 317 (1997).
[19] H. J. Reyher, H. Bauer, C. Huber, R. Mayer, A. Schäfer, and A. Winnacker, Phys. Lett. A **115**, 238 (1986).
[20] I. Baumann, M. Foerste, K. Layer, G. zu Putlitz, B. Tabbert, and C. Zühlke, J. Low Temp. Phys. **110**, 213 (1998).
[21] B. Tabbert, M. Beau, H. Günther, W. Häu$\beta$ler, C. Hönninger, K. Meyer, and G. zu Putlitz, Z. Phys. B: Condens. Matter **97**, 425 (1995).
[22] Y. Moriwaki and N. Morita, Eur. Phys. J. D **13**, 11 (2001).
[23] MOLPRO is a package of *ab initio* programs written by H.-J. Werner and P. J. Knowles.
[24] Y. Moriwaki, Y. Matsuo, and N. Morita (unpublished).
[25] M. D. Feit, J. A. Fleck, Jr., and A. Steiger, J. Comput. Phys. **47**, 412 (1982).
[26] Y. Fukuyama, Y. Moriwaki, and Y. Matsuo (unpublished).
[27] Y. Moriwaki, Y. Matsuo, and N. Morita, J. Phys. B **33**, 5099 (2000).
[28] H. J. Andrä, in *Beam–Foil Sectroscopy*, edited by I. A. Sellin and D. J. Pegg (Plenum, New York, 1976), Vol. 2, p. 835.
[29] M. Hawley and M. A. Smith, J. Chem. Phys. **95**, 8662 (1991).
[30] M. Kriegl, R. Richter, P. Tosi, W. Federer, W. Lindinger, and E. E. Ferguson, Chem. Phys. Lett. **124**, 583 (1986).
[31] R. Richter, W. Lindinger, and E . E. Ferguson, J. Chem. Phys. **89**, 5692 (1988).
[32] W. Singer, A. Hansel, A. Wisthaler, W. Lindinger, and E. E. Ferguson, Int. J. Mass. Spectrom. **223-224**, 757 (2003).